Biomaterials 35 (2014) 3934–3944

Contents lists available at ScienceDirect

Biomaterials

journal homepage: www.elsevier.com/locate/biomaterials

The effects of actin cytoskeleton perturbation on keratin intermediate filament formation in mesenchymal stem/stromal cells

Tzu-Hao Chang [a,1], Hsien-Da Huang [b,c,1], Wei-Kee Ong [d], Yun-Ju Fu [d], Oscar K. Lee [e], Shu Chien [f,g], Jennifer H. Ho [d,h,i,*]

[a] Graduate Institute of Biomedical Informatics, College of Medical Science and Technology, Taipei Medical University, Taipei, Taiwan
[b] Institute of Bioinformatics and Systems Biology, National Chiao Tung University, Hsinchu, Taiwan
[c] Department of Biological Science and Technology, National Chiao Tung University, Hsinchu, Taiwan
[d] Center for Stem Cell Research, Wan Fang Hospital, Taipei Medical University, Taipei, Taiwan
[e] Institute of Clinical Medicine, National Yang-Ming University, Taipei, Taiwan
[f] Institute of Engineering in Medicine, University of California at San Diego, La Jolla, CA, USA
[g] Departments of Bioengineering and Medicine, University of California at San Diego, La Jolla, CA, USA
[h] Graduate Institute of Clinical Medicine, Taipei Medical University, Taipei, Taiwan
[i] Department of Ophthalmology, Wan Fang Hospital, Taipei Medical University, Taipei, Taiwan

ARTICLE INFO

Article history:
Received 22 September 2013
Accepted 10 January 2014
Available online 7 February 2014

Keywords:
Chromosome 17q21.2
F-actin depolymerization
Intermediate filaments
Keratin
Mesenchymal stem cells (MSCs)
NK2 homeobox 5 (NKX2.5)

ABSTRACT

F-actin plays a crucial role in composing the three-dimensional cytoskeleton and F-actin depolymerization alters fate choice of mesenchymal stem/stromal cells (MSCs). Here, we investigated differential gene expression and subsequent physiological changes in response to F-actin perturbation by latrunculin B in MSCs. Nineteen genes were down-regulated and 27 genes were up-regulated in the first 15 min after F-actin depolymerization. Functional enrichment analysis revealed that five genes involved in keratin (KRT) intermediate filaments clustering in the chromosome 17q21.2 region, i.e., KRT14, KRT19, KRT34, KRT-associated protein (KRTAP) 1-5, and KRTAP2-3, were strongly up-regulated. Transcription factor prediction identified NKX2.5 as the potential transcription factor to control KRT19, KRT34, KRTAP1-5, and KRTAP2-3; and indeed, the protein level of NKX2.5 was markedly increased in the nuclear fraction within 15 min of F-actin depolymerization. The peak of keratin intermediate filament formation was 1 h after actin perturbation, and the morphological changes showed by decrease in the ratio of long-axis to short-axis diameter in MSCs was observed after 4 h. Together, F-actin depolymerization rapidly triggers keratin intermediate filament formation by turning on keratin-related genes on chromosome 17q21.2. Such findings offer new insight in lineage commitment of MSCs and further scaffold design in MSC-based tissue engineering.

1. Introduction

Actin filaments, microtubules and intermediate filaments are the three major types of protein filaments that form the cytoskeleton in mammalian cells. Formation of cytoskeletal filaments is dynamic in eukaryotic cells, and the cytoskeletal arrangement needs to be reorganized to attain different physical properties [1] Polymerized actin filaments (F-actins) are composed of two-stranded helical polymers of actin monomers (G-actin). The self-assembly and dynamic structures of cytoskeletal filaments contribute to the control of cell migration, proliferation, and shape stability [2]. The organization of the F-actin network maintains the 3-dimensional cell structure that delivers signals from the extracellular matrix (ECM) via integrin-actin connections [3] and signals from the cell–cell junctions via cadherin-actin complexes [4]. F-actins are sensitive to mechanical forces [5], and patterning of the actin cytoskeleton is crucial for morphological events during development such as tissue orientation, vasculogenesis, and stem cell differentiation [6].

Engineering of the biomaterials in the scaffold to guide the fate determination of stem cells through cell–matrix interaction by regulating integrin signals and actin cytoskeleton organization has been an attractive approach to offer proper cues for the cells seeded into the scaffold constructs [7,8]. Actin cytoskeleton reorganization can be achieved by F-actin depolymerization first

* Corresponding author. Graduate Institute of Clinical Medicine, Taipei Medical University, 250 Wu-Hsing Street, Taipei 110, Taiwan. Tel.: +886 2 29307930x2946; fax: +886 2 29342285.
E-mail address: wh9801@yahoo.com.tw (J.H. Ho).
[1] Tzu-Hao Chang and Hsien-Da Huang contributed equally to this work.

0142-9612/$ – see front matter © 2014 Elsevier Ltd. All rights reserved.
http://dx.doi.org/10.1016/j.biomaterials.2014.01.028

Table 1
Primers for real-time reverse transcription-polymerase chain reaction.

Gene	Primer sequence		Produce (bp)
Runx2	F: 5′-GTGCCTAGGCGCATTTCA-3′	R: 5′-GCTCTTCTTACTGAGAGTGGAAGG-3′	78
C/EBPβ	F: 5′-CGCTTACCTCGGCTACCA-3′	R: 5′-ACGAGGAGGACGTGGAGAG-3′	65
PPARr	F: 5′-TCCATGCTGTTATGGGTGAA-3′	R: 5′-TGTCAACCATGGTCATTTC-3′	113
MMP2	F: 5′-TGAAGCACAGCAGGTCTCAG-3′	R: 5′-GTGTTCAAACCAGGCACCTC-3′	71
MMP9	F: 5′-TGTACCGCTATGGTTACACTCG-3′	R: 5′-GCCCCAGAGATTTCGACTC-3′	60
ERK1	F: 5′-CCCTAGCCCAGACAGACATC-3′	R: 5′-GCACAGTGTCCATTTTCTAACAGT-3′	94
ERK2	F: 5′-CAAAGAACTAATTTTTGAAGAGACTGC-3′	R: 5′-TCCTCTGAGCCCTTGTCCT-3′	81
RhoA	F: 5′-CAGAAAAGTGGACCCCAGAA-3′	R: 5′-TGCCTTCTTCAGGTTTCACC-3′	147
ROCK1	F: 5′-CCCTCGAACGCTTTCTACA-3′	R: 5′-CACAGGGCACTCAGTCACAT-3′	104
ROCK2	F: 5′-TCAGTGGCATTGGGATAACAT-3′	R: 5′-TGCTGTCTATGTCACTGCTGAG-3′	74
KRT14	F: 5′-TGGATCGCAGTCATCCAGAG-3′	R: 5′-ATCGTGCACATCCATGACCTT-3′	73
KRT19	F: 5′-CAGCTTCTGAGACCAGGGTT-3′	R: 5′-GACTGGCGATAGCTGTAGGA-3′	70
KRT34	F: 5′-TTAACCGCAGGGAAGTGGAGC-3′	R: 5′-GCTGGATACCACCTGCTTGTT-3′	71
KRTAP1-5	F: 5′-CCACCTCTGGACCACTAACAA-3′	R: 5′-GTCCCCAGTGAAGGGTCAAG-3′	126
KRTAP2-3	F: 5′-AGCTGATCCTCAAGCACGAA-3′	R: 5′-GAGAGGGCCAGGATTAGCTG-3′	80
18S rRNA	F:5′-ATGGCCGTTCTTAGTTGGTG-3′	R:5′-AACGCCACTTGTCCCTCTAA-3′	132

Runx2, runt-related transcription factor 2; C/EBPβ, CCAAT-enhancer-binding protein beta; PPARγ, peroxisome proliferator-activated receptor gamma; MMPs, matrix metalloproteinases; ERKs, extracellular signal-regulated kinases; RhoA, Ras homolog gene family, member A; ROCKs, Rho-associated, coiled-coil containing protein kinases; KRTs, keratins; KRTAPs, keratin-associated proteins.

and subsequent re-arrangement. Latrunculin B (LAB) is a G-actin sequestering molecule, which is membrane permeable and binds to monomor G-actin to prevent F-actin assembly [9,10]. LAB causes the concentration-dependent disruption of the F-actin, and enables the investigation of the effects of F-actin depolymerization. However, F-actin depletion-induced cell death may be a consequence of high concentration treatment of LAB [11].

Mesenchymal stem/stromal cells (MSCs) are fibroblast-like adherent cells that possess multiple differentiation capacities [12,13]. It is well known that MSCs undergo spontaneous

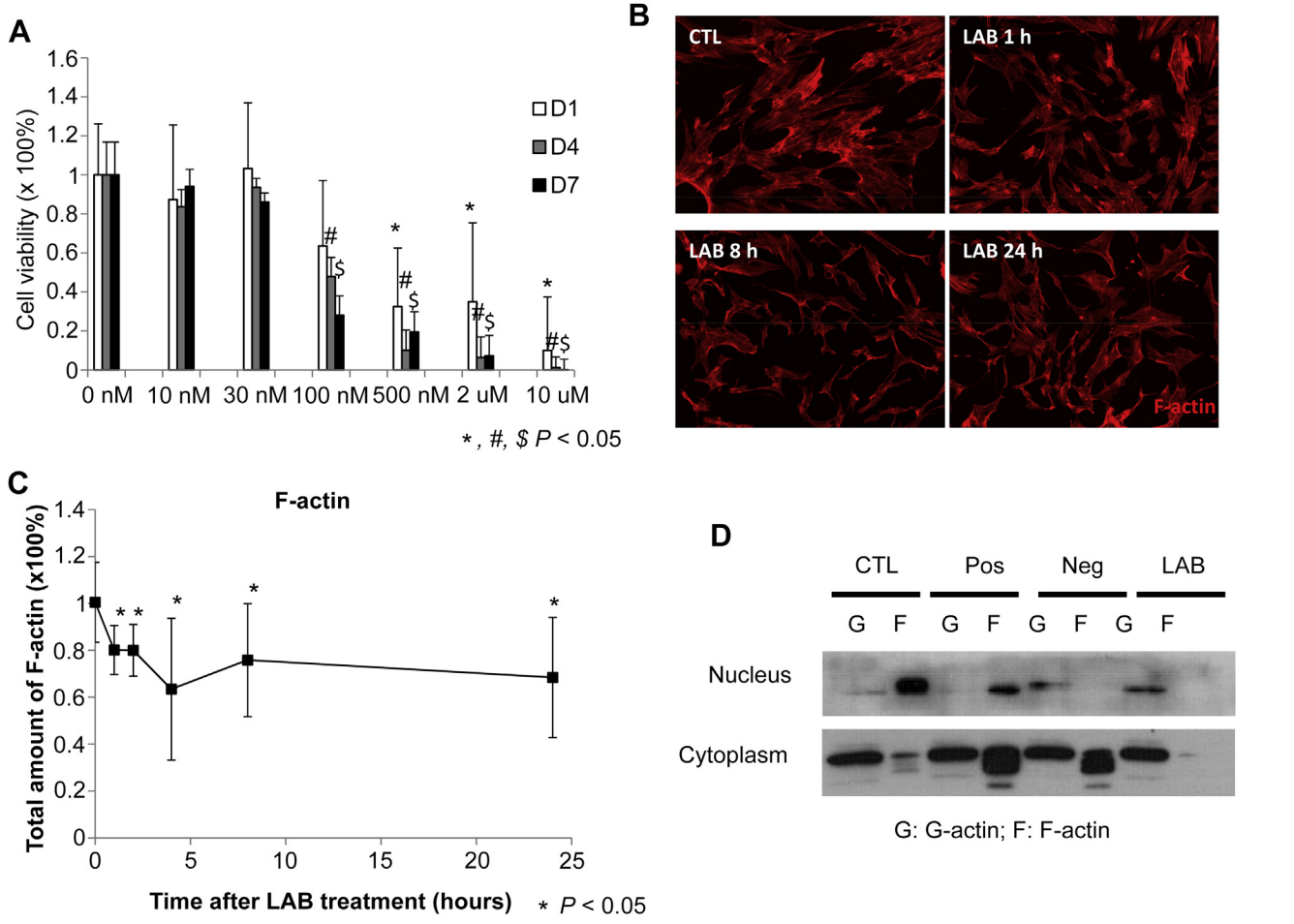

Fig. 1. Depolymerization of F-actin by latrunculin B (LAB). (A) 24-h treatment with LAB at up to 100 nM did not affect the viability of mesenchymal stem cells (MSCs), and 30 nM of LAB and below did not alter MSC viability in the first 7 days. (*, #, $ $p < 0.05$, $n = 3$) (B) LAB (30 nM) altered the shape of MSCs and the arrangement of F-actin in fibroblast-like MSCs. (C) Total amount of F-actin in MSCs was significantly decreased after 1 h of LAB (30 nM) treatment. (*$p < 0.05$, $n = 6$) (D) LAB (30 nM for 1 h) significantly disrupted F-actin in both the nucleus and cytoplasm.

differentiation in response to physical cues in the environment, such as matrix stiffness [14], the shape/size of a cell chamber, and mechanical forces [15]. The actin cytoskeleton in MSCs is composed of a large number of thin, parallel microfilament bundles that extend across the entire cytoplasm [16,17], and F-actin depolymerization is known to alter the tri-linage differentiation ability of MSCs [17–21]. We previously report that a decrease in F-actin formation in MSCs by thymosin beta-4, a F-actin sequestering peptide, results in a delay in osteogenic differentiation. Under adipogenic induction, however, a decrease in F-actin formation in MSCs accelerated maturation of adipocytic differentiation. F-actin depolymerization-induced alteration of differentiation is independent of differentiation regulation initiated by a fate-determining transcriptional factors (TFs) [18].

Although alteration of the differentiation potential is a consequence of actin cytoskeletal perturbations in MSCs, the most sensitive genes and how MSCs immediately react to the event of F-actin depolymerization are still unclear. In addition, interactions among different types of cytoskeletal responses to actin depolymerization in MSCs have not been reported. The aim of this study is to investigate the initial responses of MSCs upon actin cytoskeleton perturbation. We hypothesize that actin depolymerization, a physical stress for a cell, may rapidly regulate gene expressions, and which leads to the morphological change and alteration of differentiation potential in MSCs. Latrunculin B (LAB) is used to trigger actin depolymerization in this study.

2. Materials and methods

2.1. Isolation and culture of MSCs

MSCs from human orbital fat tissues were isolated and culture expanded as described previously [22]. All the samples were used with the informed consent of subjects, and the approval from the Institutional Review Board of TMU-Wan Fang Hospital has been obtained prior to the commencement of the study. Adipose tissues removed from the orbital cavity were fragmented, digested, and filtered. After the removal of fluid by centrifugation, cells from the resulting pellet were plated in non-coated tissue culture flasks (BD Biosciences, Franklin Lakes, NJ, USA) and maintained in Mesen Pro Medium (Invitrogen, Carlsbad, CA, USA).

2.2. Induction of actin depolymerization by LAB

Cells were seeded in 96-well tissue culture plates at a concentration of 1×10^4 cells/100 μl/well. Subsequently, the cells were treated with serial concentrations of LAB. After 1, 4, or 7 days of incubation, cell viability of each cell line was determined by an MTT colorimetric assay (Sigma–Aldrich, St. Louis, MO, USA). Cell viabilities were determined as a percentage of the untreated control.

Cells with serial concentrations of LAB treatment were stained by TRITC-labeled phalloidin (1: 100, Sigma–Aldrich), and G-actin was quantified by a Western blot analysis. The concentration of LAB (30 nM) that significantly decreased F-actin formation without cytotoxicity was determined for use in the induction of actin depolymerization.

2.3. Image quantification of F-actin and cell shape

Total amount of f-actin in a confocal image were measured using HSB approach of ImageJ [23] with the brightness threshold set to 100, and the percentage of coverage area was calculated for comparison of the changes of f-actin after LAB. More than six confocal images in each condition were measured. The long-axis and short-axis diameter of cells were manually marked, and the length was measured by

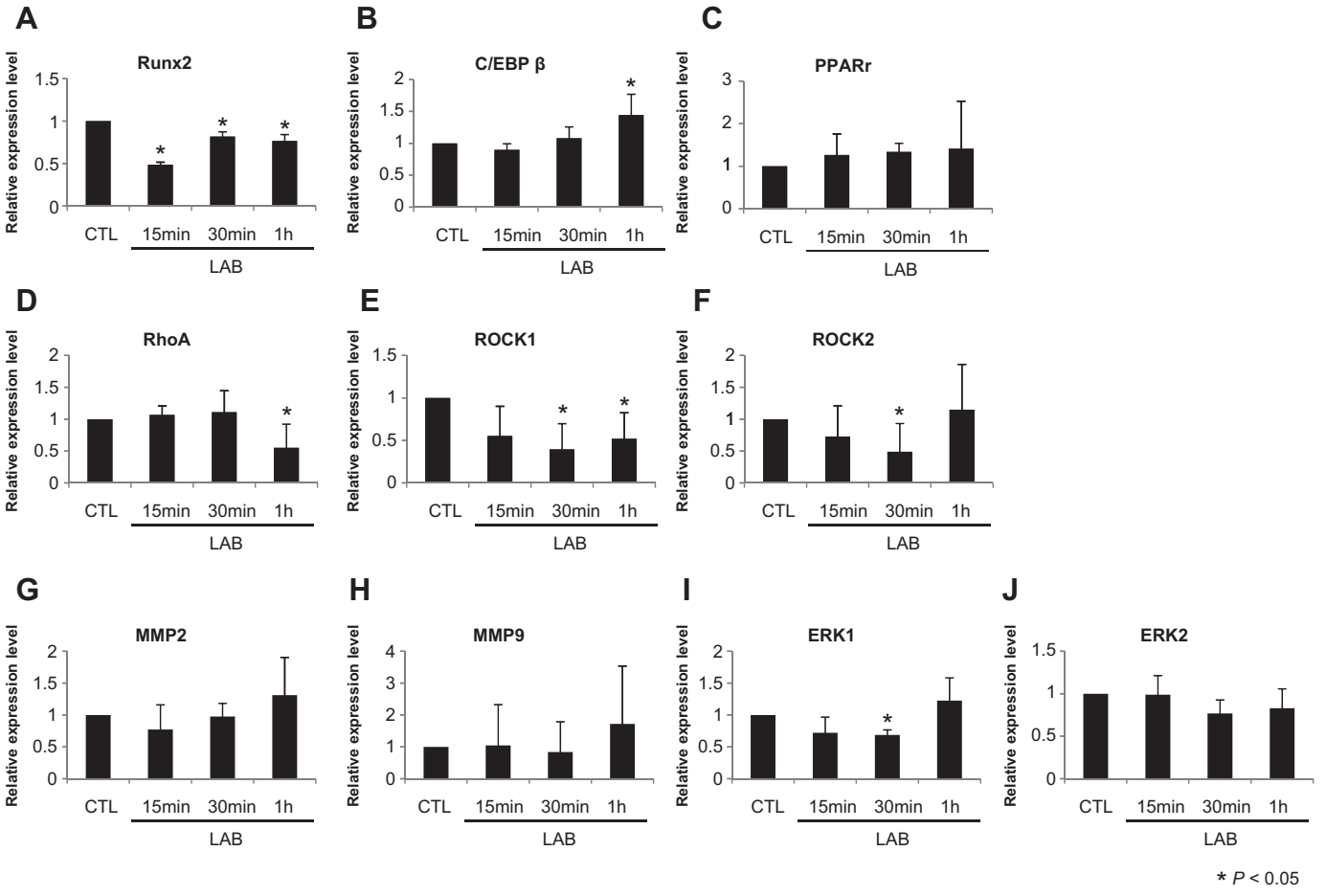

Fig. 2. Responses of fate-determining genes and actin-associated genes to actin depolymerization in mesenchymal stem cells (MSCs). During the first hour of latrunculin B (LAB) treatment, gene expression of runt-related transcription factor 2 (Runx2) significantly decreased (A), while that CCAAT-enhancer-binding protein beta (C/EBPβ) had increased at the end of 1 h (B) rather than peroxisome proliferator-activated receptor gamma (PPARγ) (C). The Ras homolog gene family member A (RhoA) (D), Rho-associated, coiled-coil containing protein kinase (ROCK)1 (E), and ROCK2 (F) decreased 30 min after LAB treatment. Matrix metalloproteinase (MMP)-2 (D) and MMP-9 (E) were not altered by LAB in the first hour. Extracellular signal-regulated kinase (ERK)1 (F), but not ERK2 (G), was transiently decreased by LAB at 30 min ($^*p < 0.05$, $n = 3$).

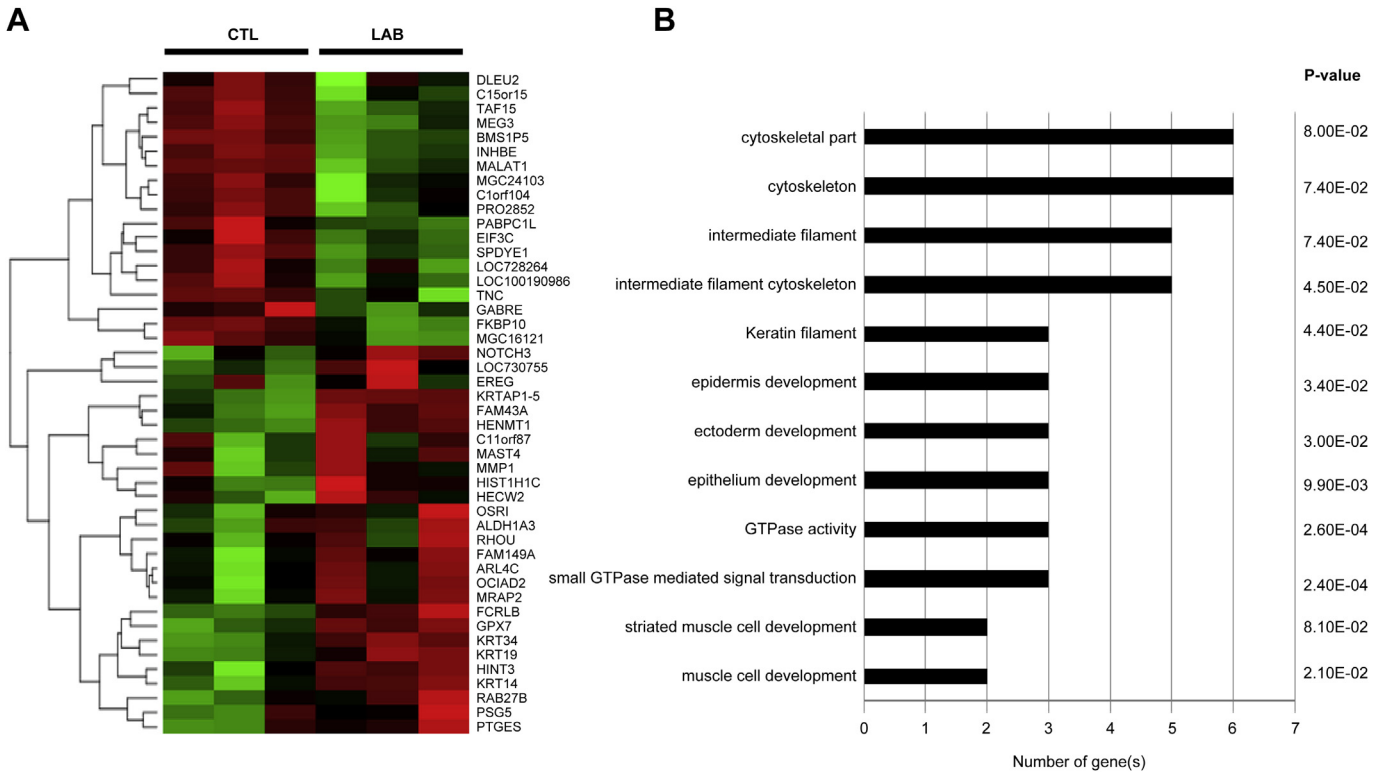

Fig. 3. Functional grouping of differentially expressed genes (DEGs) triggered by actin depolymerization. A microarray was used to analyze DEGs in mesenchymal stem cells (MSCs) before and after latrunculin B (LAB) treatment for 15 min. Nineteen DEGs were significantly down-regulated and 27 DEGs were markedly up-regulated by F-actin depolymerization (A). Functional grouping of these DEGs revealed that most genes were involved in the cytoskeleton and intermediate filaments, especially keratin filaments. Several DEGs involved in the epidermis, ectoderm, and epithelium were also rapidly regulated by LAB (B).

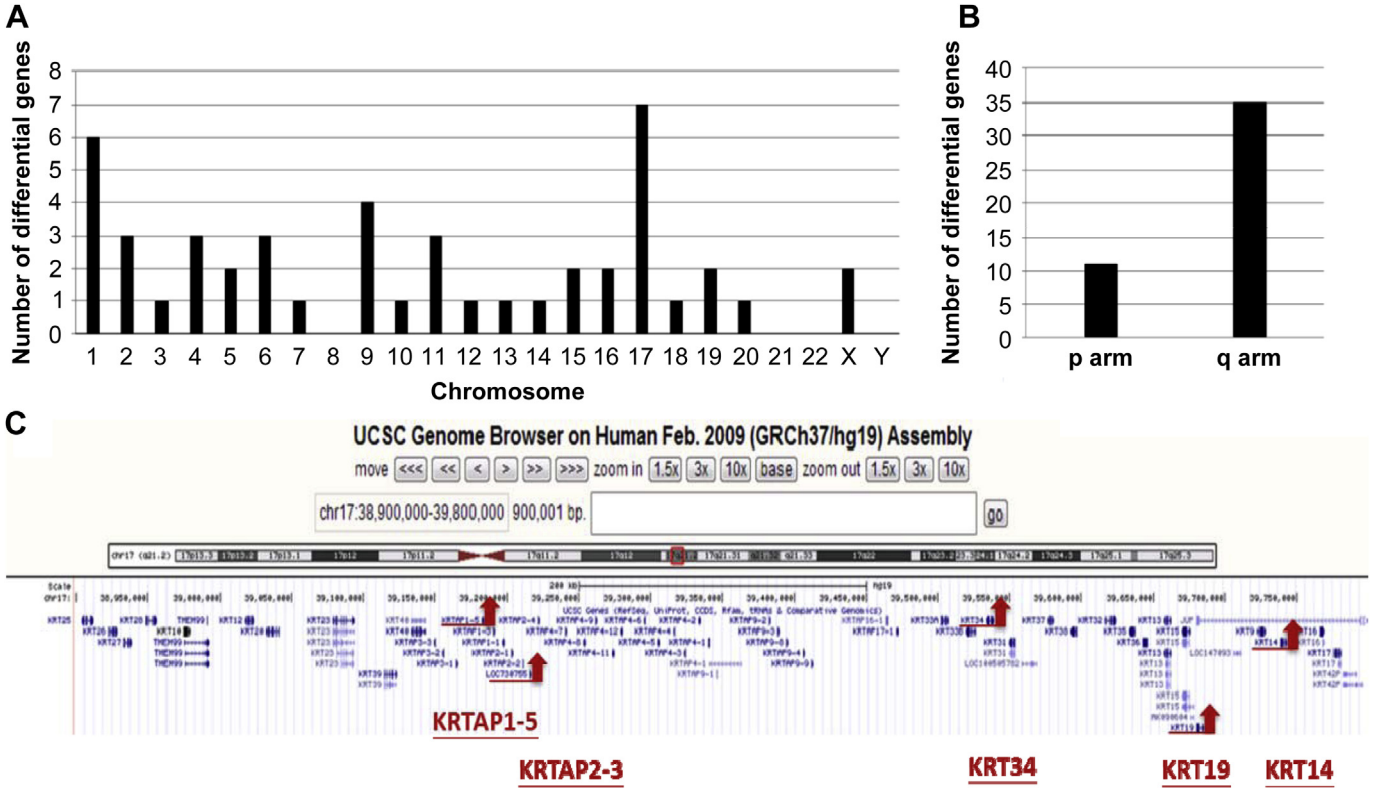

Fig. 4. Analysis of chromosome location of differentially expressed genes (DEGs). (A) A chromosome distribution analysis revealed that seven DEGs are on chromosome 17, six on chromosome 1, and four on chromosome 9. (B) Chromosome locations of DEGs showed that 35 genes are located on the q arm and 11 on the p arm. (C) The top five DEGs upregulated by LAB, i.e., keratin (KRT)14, KRT19, KRT34, keratin-associated protein (KRTAP)1-5, and KRTAP2-3, were clustered in an area of chromosome 17q21.2.

ImageJ. The ratio of long- to short-axis diameter in a cell was calculated for comparison of the changes in shapes of MSCs after LAB treatment. Twenty cells and above in each condition were marked in this experiment.

2.4. Microarray data processing

Gene profiling was performed in MSCs with or without LAB treatment for 15 min using an Affymetrix U133A 2.0 array (Affymetrix, Santa Clara, CA, USA). Three independent experiments were performed for the microarray analysis. Gene expressions in MSCs were analyzed over 20,000 annotated *Homo sapiens* gene probes. Image acquisition and probe quantification were performed using Affymetrix GeneChip Operating Software. Microarray quality control was performed using R package *affyQCReport* [24]. The *gcrma* function of R package *affy* was applied to normalize CEL files using the RMA method [25].

2.5. Identification of actin depolymerization-sensitive genes and functional analysis

Actin depolymerization-sensitive genes were defined as genes with more than 2-fold differential expression in all three paired samples between LAB treated and untreated control. All of these were considered to be differentially expressed genes (DEGs). A gene set enrichment analysis (GSEA) was performed using the Database for Annotation, Visualization and Integrated Discovery (DAVID) [26] for the Gene Ontology (GO) analysis, pathway analysis, transcription factor analysis, etc.

2.6. Quantitative real-time reverse-transcription polymerase chain reaction (RT-PCR)

The putative target genes after the functional enrichment analysis were confirmed by a real-time RT-PCR. Total RNAs were reverse-transcribed into complementary (c) DNAs using an Omniscript RT kit (Qiagen, Hilden, Germany). A real-time RT-PCR was performed using an SYBR supermix kit (Bio-Rad, Hercules, CA, USA). Samples were subjected to 40 cycles of 95 °C for 15 s, followed by 60 °C for 30 s and 72 °C for 30 s. An 18S rRNA primer was included in every plate as an internal loading control. The messenger (m)RNA level of each sample for each gene was normalized against that of 18S rRNA mRNA. The relative mRNA level was determined as $2^{[(Ct/18S\ rRNA-Ct/gene\ of\ interest)]}$. Primers for the real-time RT-PCR in this study are listed in Table 1.

2.7. Western blot analysis

Equivalent amounts of cell lysate were resolved by 10% sodium dodecylsulfate polyacrylamide gel electrophoresis (SDS-PAGE) and transferred to polyvinylidene difluoride (PVDF) membranes. After blocking, the membranes were incubated with a rabbit polyclonal antibody against G-actin (1: 500, Cytoskeleton, Denver, CO, USA) and a mouse monoclonal antibody against α-tubulin (1: 10^4, Sigma–Aldrich), NK2 homeobox 5 (NKX2.5) (1: 100, Santa Cruz, Santa Cruz, CA, USA), or activator protein 2 gamma (AP2γ) (1: 100, Abcam, Cambridge, UK) for 1 h. Membranes were then respectively treated with a goat anti-rabbit peroxidase-conjugated antibody (1:5000, Santa Cruz) and goat anti-mouse peroxidase-conjugated antibody (1:5000, Santa Cruz), and the immunoreactive proteins were detected using an enhanced chemiluminescence kit (Pierce, Rockford, IL, USA) according to the manufacturer's instructions.

2.8. Immunofluorescence staining

Cells were seeded on cover slips at a density of 3×10^5 cells per well in 6-well plates. The cells were fixed, and nonspecific antibody binding sites were blocked by incubating with 1% bovine serum albumin (BSA) in phosphate-buffered saline (PBS) at 37 °C for 1 h. Further, cells were incubated for 1 h at 37 °C with TRITC-labeled phalloidin (1: 100, Sigma–Aldrich) and a mouse monoclonal antibody against human pan-keratin (1: 25, Abcam), followed by a 1:100 dilution of a DyLight 488-conjugated secondary antibody. Then, the cover slips were incubated with DAPI for nuclear staining. Images were taken using a Zeiss LSM 410 confocal microscope (Carl Zeiss, Thornwood, NY, USA).

2.9. Statistical analysis

Statistical analyses were performed using the Statistical Package for Social Science software (vers. 16, SPSS, Chicago, IL, USA). Differences in viability without and with LAB treatment at each concentration, gene expressions, total amount of F-actin or the ratio of long- to short-axis diameter in a cell without and with LAB treatment at each time point were performed by ANOVA tests; the F values showing statistical significance ($p < 0.05$) were further analyzed with post-hoc tests; and Student's *t*-test was used for post-hoc test of different time points after LAB treatment as compared to the control samples.

3. Results

3.1. F-Actin and cell shape in MSCs after LAB treatment

The concentration of LAB in this study was determined to be that which triggered actin depolymerization in MSCs without affecting their viability [27]. Since it is known that the doubling time of MSCs is 2–3 days [22,28], the relative viabilities of MSCs treated with various concentrations of LAB were measured at 1, 4 and 7 days. MSC viability was significantly reduced by LAB at ≥500 nM after 1 day and at ≥100 nM after 4 and 7 days, but it was not altered by ≤30 nM of LAB up to 7 days (Fig. 1A). Based on these findings, 30 nM of LAB was chosen for subsequent experiments. Under confocal microscopic observation and quantification F-actin signals in confocal images, F-actin consisted of long fibers with a multidirectional distribution in MSCs in undifferentiated medium (Fig. 1B, CTL). Treatment with 30 nM of LAB for 1 h and longer markedly decreased F-actin signals in MSCs (Fig. 1C), and the morphological change was not significant at 1 h (Fig. 1B, LAB 1 h). After 8 and 24 h of LAB treatment, change of cell shape was obviously (Fig. 1B, LAB 8 h and 24 h). The Western blot analysis demonstrated that 30 nM of LAB for 1 h significantly disrupted F-actin in MSCs in both the nucleus and the cytoplasm (Fig. 1D).

3.2. Actin cytoskeleton- and fate-determined gene expressions

In our previous work, we demonstrated that F-actin depolymerization inhibited osteogenic differentiation and facilitated adipogenic differentiation of MSCs during the first week of

Table 2
List of up-regulated genes after LAB treatment for 15 min.

Gene	Log_2FoldChange	Chromosome	Location
KRTAP1-5	**4.301**	**17,**	**q21.2**
KRT14	**3.049**	**17,**	**q21.2**
KRTAP2-3	**2.979**	**17,**	**q21.2**
KRT34	**2.912**	**17,**	**q21.2**
KRT19	**2.838**	**17,**	**q21.2**
HINT3	2.67	6,	q22.32
MMP1	2.344	11,	q22.2
EREG	2.084	4,	q13.3
RAB27B	2.063	18,	q21.2
GPX7	2.016	1,	p32.3
ALDH1A3	1.833	15,	q26.3
HIST1H1C	1.699	6,	p22.2
HECW2	1.566	2,	q32.3–q32.1
C11orf87	1.547	11,	q22.3
HENMT1	1.542	1,	p13.3
FCRLB	1.534	1,	q23.3
RHOU	1.484	1,	q42.13
NOTCH3	1.422	19,	p13.12
PSG5	1.391	19,	q13.31
MAST4	1.377	5,	q12.3
FAM43A	1.375	3,	q29
OSR1	1.356	2,	p24.1
FAM149A	1.311	4,	q35.1
MRAP2	1.181	6,	q14.2
PTGES	1.143	9,	q34.11
ARL4C	1.124	2,	q37.1
OCIAD2	1.097	4,	p11

The bold values are the top 5 up-regulated genes by LAB.
KRTAP1-5, keratin associated protein 1-5; KRT14, keratin 14; KRTAP2-3, keratin associated protein 2-3; KRT34, keratin 34; KRT19, keratin 19; HINT3, histidine triad nucleotide binding protein 3; MMP1, matrix metalloproteinase 1; EREG, epiregulin; RAB27B, Rab-27B; GPX7, glutathione peroxidase 7; ALDH1A3, aldehyde dehydrogenase 1 family, member A3; HIST1H1C, histone cluster 1, H1c; HECW2, HECT, C2 and WW domain containing E3 ubiquitin protein ligase 2; C11orf87, chromosome 11 open reading frame 87; HENMT1, HEN1 methyltransferase homolog 1; FCRLB, Fc receptor-like B; RHOU, ras homolog family member U; NOTCH3, Neurogenic locus notch homolog protein 3; PSG5, Pregnancy-specific beta-1-glycoprotein 5; MAST4, Microtubule Associated Serine/Threonine Kinase Family Member 4; FAM43A, family with sequence similarity 43, member A; OSR1, oxidative-stress responsive 1; FAM149A, family with sequence similarity 149, member A; MRAP2, melanocortin 2 receptor accessory protein 2; PTGES, prostaglandin E synthase; ARL4C, ADP-ribosylation factor-like 4C; OCIAD2, OCIA domain containing 2.

induction [18]. In the current study, we found that expression of the runt-related transcription factor 2 (Runx2) gene, a fate-determining TF for osteogenic differentiation, was inhibited by LAB in the first hour (Fig. 2A). Two TFs of adipogenic differentiation, i.e., CCAAT-enhancer-binding protein beta (C/EBPβ) and peroxisome proliferator-activated receptor gamma (PPARγ) were also measured. C/EBPβ responded to LAB within 1 h (Fig. 2B), while PPARγ was not altered in the first hour of LAB treatment (Fig. 2C).

The Ras homolog gene family member A (RhoA) and its effector proteins of Rho-associated coiled-coil containing protein kinases (ROCKs) regulate the actin cytoskeleton through the formation of stress fibers [29]. In addition, matrix metalloproteinases (MMPs), especially MMP-2 and -9 [30,31], and extracellular signal-regulated kinases (ERKs) [32] are reactive to actin cytoskeleton reorganization and morphological changes. We showed that gene expressions of RhoA (Fig. 2D) and ROCK1 (Fig. 2E) in MSCs were inhibited by LAB at 1 h, while ROCK2 (Fig. 2F) showed only a transient response to LAB at 30 min. Gene expressions of MMP-2 (Fig. 2G), MMP-9 (Fig. 2H), and ERK2 (Fig. 2J) were not altered, while ERK1 (Fig. 2I) was transiently inhibited by LAB at 30 min.

3.3. Differentially expressed genes after F-actin depolymerization

To determine which effector genes immediately respond to F-actin depolymerization, a microarray analysis of MSCs before and 15 min after LAB treatment was performed. The 2-fold up- or down-regulated genes after LAB treatment in all three paired samples were defined as DEGs, which represent effector genes that responded to F-actin depolymerization. Among the 46 DEGs identified, the heat map graph showed that 27 of them were up-regulated, and 19 were down-regulated (Fig. 3A). Results of the gene set enrichment analysis revealed that most genes sensitive to LAB-induced F-actin depolymerization were involved in the organization of intermediate filaments, especially keratin filaments. Several genes involved with the epidermis, ectoderm, and epithelium were also rapidly up-regulated by LAB within 15 min (Fig. 3B).

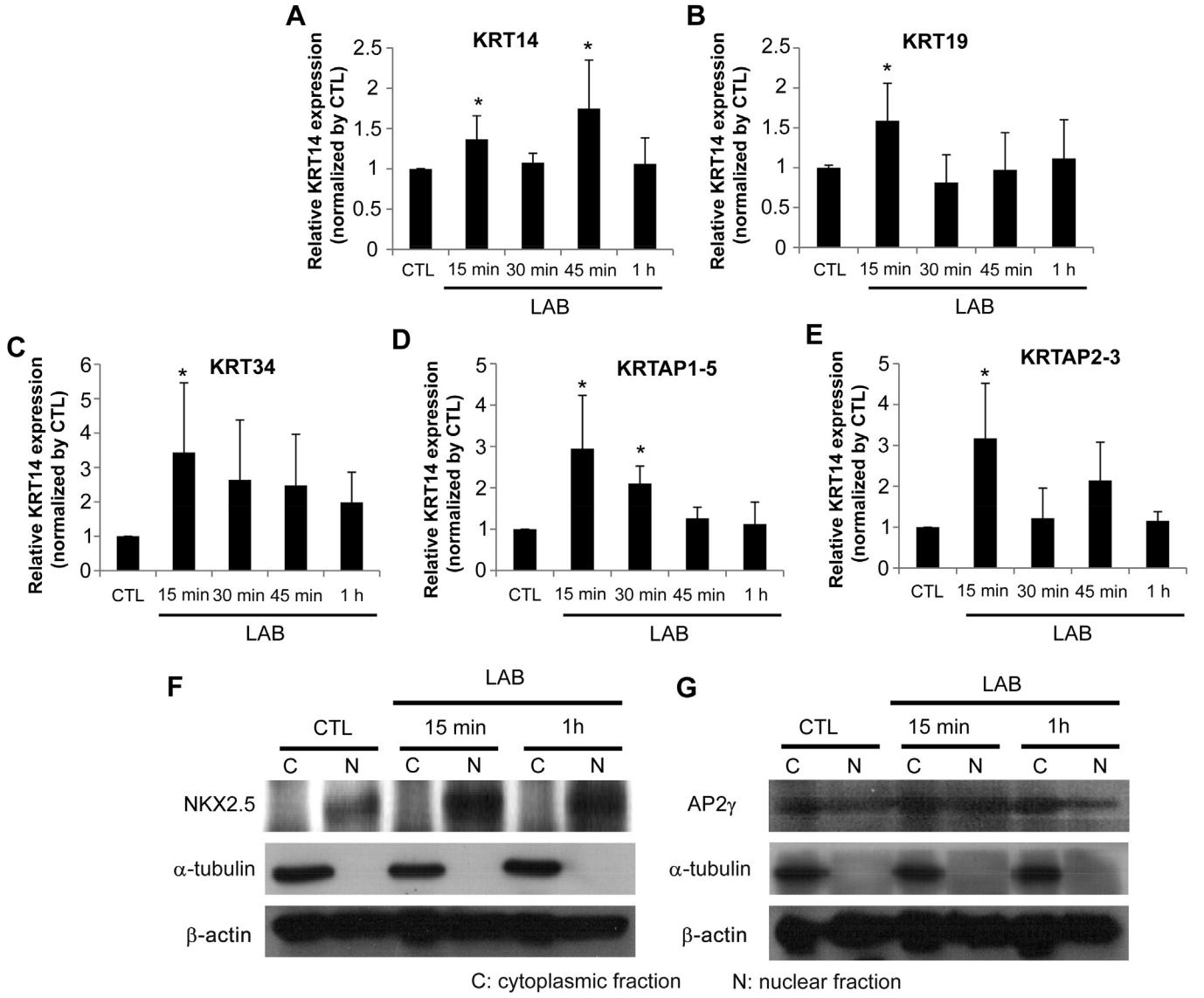

Fig. 5. Association of upregulation of genes on chromosome 17q21.2 and an increase in nuclear NKX2.5. Genes of (A) keratin (KRT)14, (B) KRT19, (C) KRT34, (D) keratin-associated protein (KRTAP)1-5, and (E) KRTAP2-3 were sensitive and transiently responsive to F-actin depolymerization. (*$p < 0.05$, $n = 3$) (F) NK2 homeobox 5 (NKX2.5), a potential transcription factor of KRT19, KRT34, KRTAP1-5, and KRTAP2-3, significantly increased in the nuclear fraction in the first 15 min. (G) Activator protein 2 gamma (AP2γ), a potential transcription factor of KRT14, KRT19, and KRT34, showed no response to latrunculin B (LAB) treatment within the first hour.

3.4. Keratin-associated DEGs cluster on chromosome 17q21.2

In addition to functional grouping by the gene set enrichment analysis, we analyzed the chromosome distribution of DEGs. Although 46 DEGs were distributed on 20 different chromosomes, chromosomes 17 and 1 were the two most sensitive chromosomes to actin perturbation (Fig. 4A). Moreover, we found that most of the DEGs were located on the q arm of the chromosomes (Fig. 4B). Notably, six up-regulated DEGs were located on 17q21.2 (Fisher extract p value = 1.1E-9), and five of these six were keratin-associated genes: keratin-associated protein 1-5 (KRTAP1-5), keratin 14 (KRT14), KRTAP2-3, KRT34, and KRT19. Using the UCSC genome browser, we identified a region of keratin-associated gene clusters from ch17:38,900,000 to 39,800,800 (Fig. 4C). Remarkably, the above-described 5 keratin-associated genes located on 17q21.2 were also the top five DEGs up-regulated by LAB (Table 2).

To confirm that the keratin-associated genes on chromosome 17q21.2 were most sensitive and most rapidly responsive to F-actin depolymerization, gene expression levels of these five keratin-associated genes in MSCs before and after LAB treatment were measured by real-time RT-PCR. The time-dependent gene expressions of KRT14 (Fig. 5A), KRT19 (Fig. 5B), KRT34 (Fig. 5C), KRTAP1-5 (Fig. 5D) and KRTAP2-3 (Fig. 5E) exhibited a similar pattern after LAB treatment. All five of these keratin-associated genes located on 17q21.2 were highly up-regulated in the first 15 min (Fig. 5A–E).

3.5. TFs associated with up-regulation of keratin genes on 17q21.2

To elucidate the key regulator that modulates the DEGs triggered by F-actin depolymerization, TF predictions were performed using the DAVID database. NKX2.5, AP2γ, c-REL, GATA6, and interferon regulatory factor 1 (IRF1) were potentially TFs by targeting the up-regulated DEGs (Table 3). The power and multiple of change of differential expression regulated by these TFs showed that NKX2.5 regulated 19 of 26 (70.4%) up-regulated DEGs, while IRF1 regulated 11 of 26 (40.7%). CREL, GATA6, and AP2γ regulated 7, 7, and 5 up-regulated DEGs, respectively (Table 4). None of the predicted TFs showed a significant alteration of gene expression according to the microarray analysis (Table 4, Log2 multiples of change of <1). Although NKX2.5 and IRF1 regulated most of the up-regulated DEGs, NKX2.5 potentially turned on four keratin-associated genes on 17q21.2, while IRF1 showed no effect on keratin-associated genes on 17q21.2 (Table 3). In addition, AP2γ only regulated five of the up-regulated DEGs, among which three were keratin-associated genes on 17q21.2 (Table 3). According to the above findings, NKX2.5 and AP2γ probably serve as potential TFs for keratin-associated genes on 17q21.2.

Western blot analysis was performed to confirm the key TFs regulating the targeted keratin-associated genes on 17q21.2. We demonstrated that NKX2.5, the potential TF for KRT19, KRT34, KRTAP1-5, and KRTAP2-3, was mainly in the nuclear fraction and increased in the nuclear fraction in the first 15 min of LAB treatment (Fig. 5F). AP2γ, the potential TF for KRT14, KRT19, and KRT34, was dominant in the cytoplasmic fraction and was not affected by LAB in the first hour (Fig. 5G).

3.6. Keratin intermediate filament formation after F-actin depolymerization

Keratins are intermediate filament-forming proteins that are abundant in epithelial tissues [33]. According to our data in Figs. 3–5 and Tables 2–4, transcriptions of genes involved in keratin-associated intermediate filaments on 17q21.2 were activated by F-actin depolymerization within 15 min. We further tested whether keratin intermediate filament formation followed F-actin depolymerization. Under confocal microscope, LAB gradually reduced F-actin signals by decreasing the thickness and length of actin filaments in MSCs in the first 4 h (Fig. 6A–D, red signals). Different from F-actin, keratin filament formation increased and peaked at 1 h after LAB treatment (Fig. 6A–C, green signals). Interestingly, keratin signals had decreased at 4 h of LAB treatment in the cytosol except for the perinuclear region (Fig. 6D, green signals). Quantification of confocal images revealed that the F value of cell shape change after LAB treatment is 2.56 (p = 0.032). The ratio of long- to short-axis diameter in MSCs was significantly decreased by LAB treatment at 4 h (p = 0.004), 8 h (p = 0.013), and 24 h (p = 0.017) (Fig. 6E–G), showing that changes of cell shape in MSCs was significant after treatment with LAB for 4 h.

Table 3
Potential transcription factors of up-regulated genes after LAB treatment.

Transcription factor	Target genes	Transcription factor	Target genes	Transcription factor	Target genes
NKX2.5	**KRTAP1-5**	**AP2γ**	**KRT14**	**c-REL**	**KRTAP2-3**
	KRTAP2-3		**KRT34**		MMP1
	KRT34		**KRT19**		ALDH1A3
	KRT19		NOTCH3		HECW2
	MMP1		MAST4		NOTCH3
	EREG				MAST4
	RAB27B				ARL4C
	ALDH1A3	**IRF1**	ARL4C		
	HECW2		HECW2		
	C11orf87		OCIAD2	**GATA6**	**KRT19**
	FCRLB		RAB27B		HECW2
	RHOU		ALDH1A3		RAB27B
	NOTCH3		HENMT1		EREG
	MAST4		C11orf87		MMP1
	OSR1		EREG		MRAP2
	FAM149A		FAM149A		MAST4
	PTGES		HIST1H1C		
	ARL4C		MAST4		
	OCIAD2				

The bold values are the top 5 up-regulated genes by LAB in MSCs.
NKX2.5, NK2 homeobox 5; AP2γ, activator protein 2 gamma; IRF1, interferon regulatory factor 1.
The shaded values are to distinguish the top 5 up-regulated genes from potential transcription factors.

4. Discussion

In this study, we explore the crosstalk between actin filaments and intermediate filaments in MSCs triggered by F-actin depolymerization, and identify NKX2.5 as a potential TF in the regulation of keratin-associated genes on chromosome 17q21.2. MSCs are fibroblast-like cells maintaining their 3-dimensional structure mainly through F-actin under normal conditions (Figs. 1B, 6A and 7A). LAB-induced rapid F-actin depolymerization increases the risk of cytoskeleton collapse and also triggers the transcriptional regulation on effector genes (Figs. 2–4, Table 2), especially the up-regulation of KRTAP1-5, KRTAP2-3, KRT14, KRT19, and KRT34 on

Table 4
Power and fold change of differential expression of NKX2.5, IRF1, c-REL, GATA6 and AP2γ.

Transcript factor	Count of target genes	Percentage (%)	*P*-value	Log2Fold Change
NKX2.5	19	70.4	8.7E-2	0
IRF1	11	40.7	3.0E-2	0.73
c-REL	7	25.9	1.2E-1	−0.01
GATA6	7	25.9	1.3E-1	−0.24
AP2γ	5	18.5	1.8E-1	0

NKX2.5, NK2 homeobox 5; AP2γ, activator protein 2 gamma; IRF1, interferon regulatory factor 1.

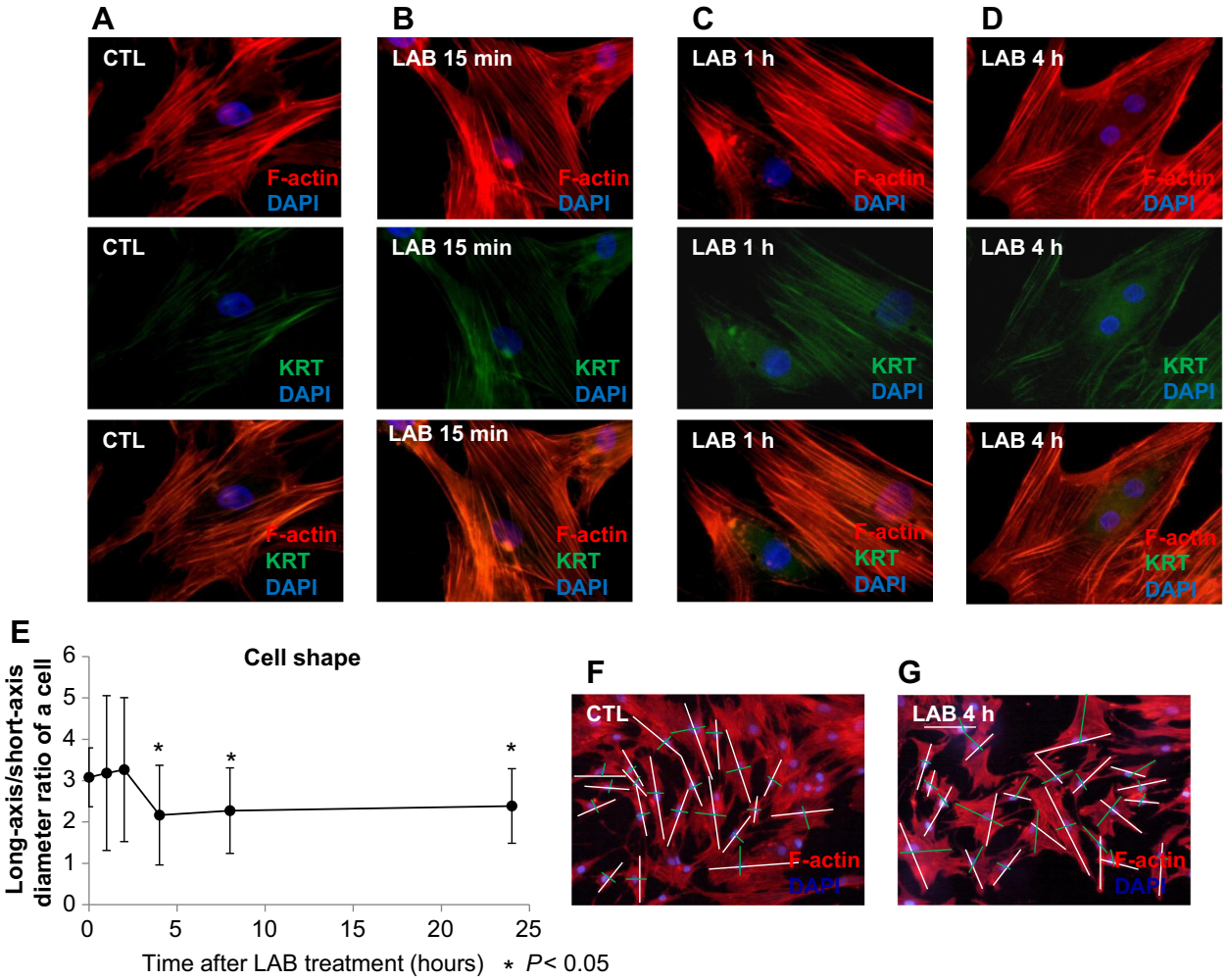

Fig. 6. Formation of keratin filaments as a consequence of F-actin depolymerization. (A–D) During the first 4 h of latrunculin B (LAB) treatment, the thickness and length of intracellular actin-filaments were progressively disrupted (red signals). (A) The signal of keratin intermediate filaments was much lower than actin filaments in mesenchymal stem cells (MSCs) under normal conditions. (B) Keratin intermediate filaments were found at the cell periphery of MSCs after treatment with LAB for 15 min. (C) One hour after LAB treatment, the periphery and perinuclear area were filled with keratin intermediate filaments. (D) Strong perinuclear keratin signals were observed in MSCs 4 h after LAB treatment. (E) The ratio of long-axis/short-axis diameter in MSCs was significantly decreased by LAB after 4 h (*$p < 0.05$, $n = 20$). (F, G) Long axis in a cell was marked with white line, while short axis was lined by green. (For interpretation of the references to color in this figure legend, the reader is referred to the web version of this article.)

17q21.2 through NKX2.5 (Figs. 5 and 7B, Tables 3 and 4). Thus, keratin intermediate filament formation replaces F-actin to compensate for the collapse of actin cytoskeleton (Fig. 6B–D, 7C).

In the cytoskeleton, F-actins act as the tension sensor [5], while intermediate filaments play a role as a mechanical stress absorber [34]. Intermediate filaments are composed of cell type-specific filament-forming proteins such as lamins in the nucleus, vimentin in fibroblasts and many cells of mesenchymal origin, desmin in muscle cells, keratins in epithelial cells and their derivations, and neurofilaments in neurons [35,36]. Intermediate filaments and their associated proteins have been found to be the major components in mediating cytoskeletal crosstalk [37]. In this study, LAB disrupted the actin cytoskeleton by depolymerizing F-actin to perturb the 3-dimensional structure of MSCs. Our results showed that keratins, rather than other intermediate filament-forming proteins, quickly responded to F-actin depolymerization in the first 15 min (Figs. 3 and 5, Table 2) and formed intermediate filaments within 1 h (Fig. 6A–D) in MSCs to prevent cell collapse. Physiologically, intermediate filament protein polymerization starts from the peripheral cell membrane to the nuclear membrane [1,38], and a time lag from the genetic expression to protein production is essential. This may be the explanation why transient keratin intermediate filament formation was observed from 1 to 4 h after LAB treatment (Fig. 6C and D), and keratin signals at perinuclear region were predominant at 4-h of treatment (Fig. 6D). With such interactions between actin filaments and intermediate filaments, MSCs maintained their viability (Fig. 1A). However, as a consequence, the morphological change occurred (Figs. 1B and 6E-G) and the fate alteration of MSCs may also be related.

In total, 54 keratins have been identified in two families, i.e., type I for acidic and type II for neutral and basic keratins [33]. Keratin intermediate filaments, which are abundant in epithelia such as that of the skin, hair, and liver, form cytoskeletal networks and maintain cell function [34,39,40]. According to our findings, KRTAP1-5, KRTAP2-3, KRT14, KRT19, and KRT34 are the most sensitive genes to F-actin depolymerization in MSCs (Figs. 3–5, Table 2). In the epidermis, KRT14 is the major keratin in basal cells of stratified epithelium and is essential for a stable and normal epidermis [33,40]. KRT19, also known as cytokeratin 19, is an epithelial stem/progenitor cell marker found in limbal progenitor cells [41], hair follicle stem cells [42], and bipotential hepatic progenitor cells [43]. KRT34 is a type I hair keratin [44], and KRTAPs are

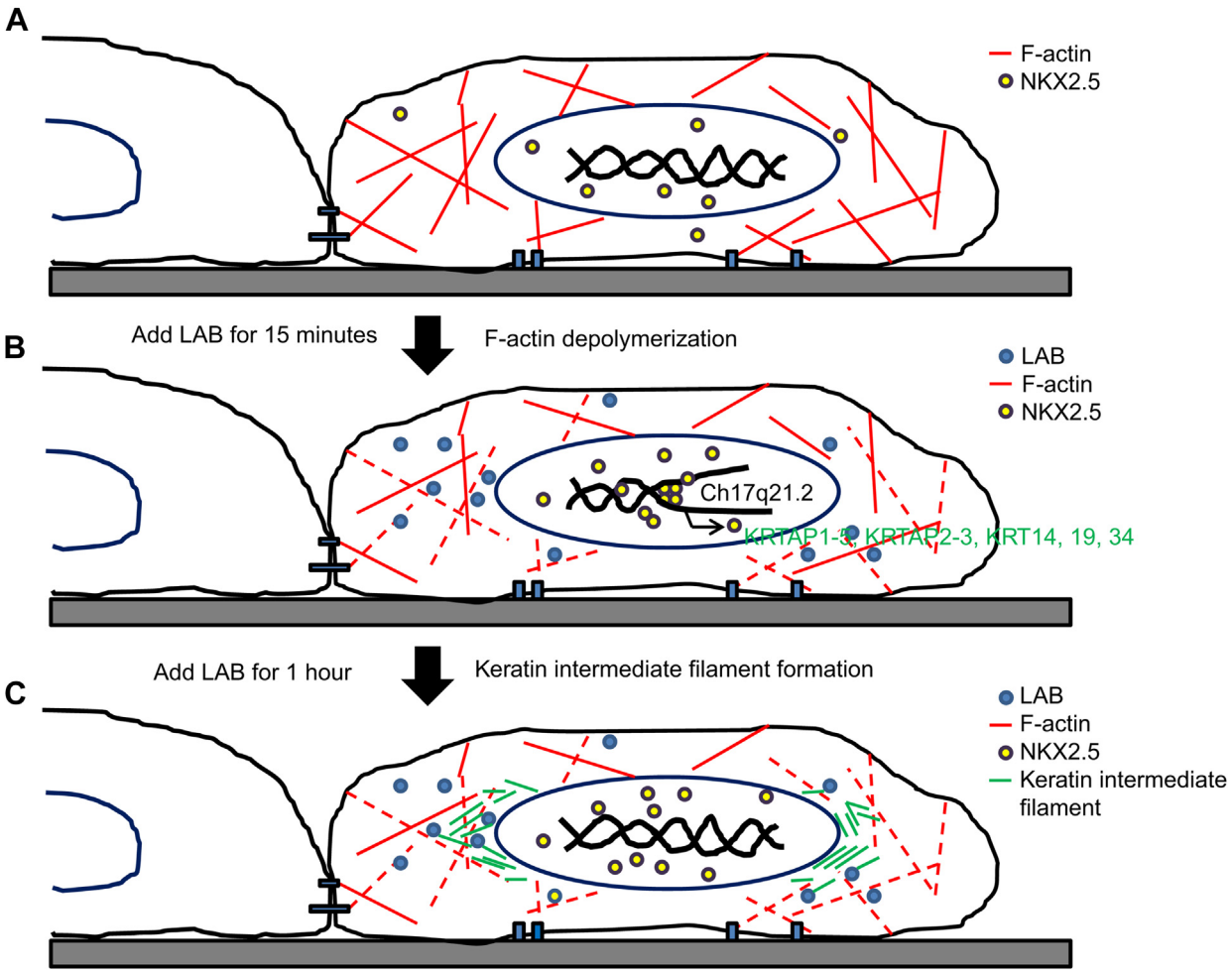

Fig. 7. Schema of this study (A) Under normal conditions, actin filaments were dominant cytoskeleton supporting the mesenchymal stem cell (MSC) structure. (B) F-actin depolymerization by LAB in MSCs triggered keratin-associated gene expressions on chromosome 17q21.2 with transcriptional regulation by NKX2.5. (C) Depolymerized actin filaments were replaced by keratin intermittent filaments to prevent collapse of the cytoskeleton, and keratin intermediate filament formation began at the cell periphery and condensed in the perinuclear area in MSCs upon F-actin depolymerization.

involved in hair follicle differentiation and regulation [45,46]. MSC transplantation is effective in promoting skin wound healing by both differentiation into KRT14-expressing cells and a paracrine effect [47–49]. Aljitawi et al. report that cytokeratin 19-positive cells with hair-like structures are generated from MSCs [50], while Hwang et al. demonstrate that transplanted MSCs *in vivo* first differentiate into cytokeratin 19-expressing oval cells and later into albumin-producing hepatocyte-like cells [51]. Recently, Shi et al. report that F-actin depolymerization triggers a mesenchymal–epithelial transition in fibroblasts [21], but little is known about MSCs. Herein, we discovered that disruption of F-actin triggered transient increases in the expressions of KRT14, KRT19, KRT34, KRTAP1-5, and KRTAP2-3 in the first hour (Fig. 5A–E), and the impacts of such changes on MSC differentiation into epithelial cells, hepatocytes, and hair follicles are being evaluated in our lab.

The chromosome 17q21.2 gene domain contains 27 type I keratin genes [52]. We demonstrated that only five genes were strongly up-regulated after actin filament perturbation (Fig. 4C), and four of them were potentially regulated by the same transcription factor, i.e., NKX2.5 (Tables 3 and 4). NKX2.5 is a well-known marker of precardiac cells that binds with GATA4 to activate the cardiac atrial natriuretic factor during cardiac development [53]. Mutation of the NKX2.5 gene is associated with congenital heart disease [54] and thyroid dysgenesis [55]. It is known that nuclear translocation of NKX2.5 and GATA4 drives the cardiac differentiation of MSCs [56]. In addition, NKX2.5 has been reported to inhibit myocyte differentiation, and the overexpression of NKX2.5 promotes neuronal cell differentiation in skeletal myoblasts [57]. In this study, we explored how F-actin depolymerization enhanced NKX2.5 in the nuclear fraction within 15 min (Fig. 5F) without altering NKX2.5 gene expression (Table 4); therefore, the transcriptional regulation of NKX2.5 by F-actin depolymerization could be ruled out. However, impacts of actin perturbation on translational and post-translational regulation of NKX2.5 in MSCs and the interaction between F-actin and NKX2.5 needs to be further investigated.

In this study, we point out that keratin intermediate filament and NKX2.5 on transcriptional regulation of chromosome 17q21.2 are putative targets for F-actin depolymerization-induced gene regulation during cytoskeleton re-organization in MSCs. Such findings can be taken into consideration for the future development of scaffolds in MSC-based tissue engineering, so that cell fate determination of the MSCs in the scaffolds can be more accurately controlled.

5. Conclusion

The increase in keratin intermediate filaments in MSCs is an immediate compensatory response to F-actin depolymerization. The interaction between actin filaments and intermediate

filaments is achieved by rapidly turning on keratin-associated genes on chromosome 17q21.2 which are potentially regulated by NKX2.5. The results of this study have unraveled critical interactions between actin filaments and keratin intermediate filaments and the regulatory mechanism of the biophysical effects initiated by F-actin depolymerization in MSCs. Such findings have provided new insight into further scaffold design in MSC-based tissue engineering.

Acknowledgments

The authors acknowledge the support of research grants from the National Science Council (NSC101-2314-B-038-022-MY3 and NSC101-2120-M-010-002 to JHH and OKL; NSC100-2911-I-010-503 to SC, OKL, and JHH; NSC100-2314-B-010-030-MY3, NSC101-2321-B-010-009, and NSC101-2911-I-010-503 to OKL). This work was also supported in part by the UST-UCSD International Center of Excellence in Advanced Bio-engineering sponsored by the Taiwanese National Science Council I-RiCE Program under grant no.: NSC101-2911-I-009-101. The authors also acknowledge the financial support from California Institute of Regenerative Medicine (CIRM RT2-01889 and RB3-05086 to SC), Wan Fang Hospital, Taipei Medical University (102swf02 to JHH and OKL; 102-TMU-WFH-05 to THC and JHH), Taipei Medical University (TMU101-AE1-B44 to THC), and a research grant support from Taipei Medical University and Steminent Biotherapeutics (A-101-023).

References

[1] Wang YL. Dynamics of the cytoskeleton in live cells. Curr Opin Cell Biol 1991;3:27–32.
[2] Vignaud T, Blanchoin L, Thery M. Directed cytoskeleton self-organization. Trends Cell Biol 2012;22:671–82.
[3] Brakebusch C, Fassler R. The integrin-actin connection, an eternal love affair. EMBO J 2003;22:2324–33.
[4] Brieher WM, Yap AS. Cadherin junctions and their cytoskeleton(s). Curr Opin Cell Biol 2013;25:39–46.
[5] Galkin VE, Orlova A, Egelman EH. Actin filaments as tension sensors. Curr Biol 2012;22:R96–101.
[6] Patwari P, Lee RT. Mechanical control of tissue morphogenesis. Circ Res 2008;103:234–43.
[7] Attia M, Santerre JP, Kandel RA. The response of annulus fibrosus cell to fibronectin-coated nanofibrous polyurethane-anionic dihydroxyoligomer scaffolds. Biomaterials 2011;32:450–60.
[8] Schagemann JC, Kurz H, Casper ME, Stone JS, Dadsetan M, Yu-Long S, et al. The effect of scaffold composition on the early structural characteristics of chondrocytes and expression of adhesion molecules. Biomaterials 2010;31:2798–805.
[9] Coue M, Brenner SL, Spector I, Korn ED. Inhibition of actin polymerization by latrunculin A. FEBS Lett 1987;213:316–8.
[10] Morton WM, Ayscough KR, McLaughlin PJ. Latrunculin alters the actin-monomer subunit interface to prevent polymerization. Nat Cell Biol 2000;2:376–8.
[11] Spector I, Shochet NR, Blasberger D, Kashman Y. Latrunculins–novel marine macrolides that disrupt microfilament organization and affect cell growth: I. Comparison with cytochalasin D. Cell Motil Cytoskeleton 1989;13:127–44.
[12] Herzog EL, Chai L, Krause DS. Plasticity of marrow-derived stem cells. Blood 2003;102:3483–93.
[13] Dominici M, Le Blanc K, Mueller I, Slaper-Cortenbach I, Marini F, Krause D, et al. Minimal criteria for defining multipotent mesenchymal stromal cells. The International Society for Cellular Therapy position statement. Cytotherapy 2006;8:315–7.
[14] Kuo SW, Lin HI, Ho JH, Shih YR, Chen HF, Yen TJ, et al. Regulation of the fate of human mesenchymal stem cells by mechanical and stereo-topographical cues provided by silicon nanowires. Biomaterials 2012;33:5013–22.
[15] Kang Y, Kim S, Khademhosseini A, Yang Y. Creation of bony microenvironment with CaP and cell-derived ECM to enhance human bone-marrow MSC behavior and delivery of BMP-2. Biomaterials 2011;32:6119–30.
[16] Costa P, Almeida FV, Connelly JT. Biophysical signals controlling cell fate decisions: how do stem cells really feel? Int J Biochem Cell Biol 2012;44:2233–7.
[17] Maloney JM, Nikova D, Lautenschlager F, Clarke E, Langer R, Guck J, et al. Mesenchymal stem cell mechanics from the attached to the suspended state. Biophys J 2010;99:2479–87.
[18] Ho JH, Ma WH, Su Y, Tseng KC, Kuo TK, Lee OK. Thymosin beta-4 directs cell fate determination of human mesenchymal stem cells through biophysical effects. J Orthop Res 2010;28:131–8.
[19] Rodriguez JP, Gonzalez M, Rios S, Cambiazo V. Cytoskeletal organization of human mesenchymal stem cells (MSC) changes during their osteogenic differentiation. J Cell Biochem 2004;93:721–31.
[20] Mathieu PS, Loboa EG. Cytoskeletal and focal adhesion influences on mesenchymal stem cell shape, mechanical properties, and differentiation down osteogenic, adipogenic, and chondrogenic pathways. Tissue Eng Part B Rev 2012;18:436–44.
[21] Shi JW, Liu W, Zhang TT, Wang SC, Lin XL, Li J, et al. The enforced expression of c-Myc in pig fibroblasts triggers mesenchymal-epithelial transition (MET) via F-actin reorganization and RhoA/Rock pathway inactivation. Cell Cycle 2013;12:1119–27.
[22] Ho JH, Ma WH, Tseng TC, Chen YF, Chen MH, Lee OK. Isolation and characterization of multi-potent stem cells from human orbital fat tissues. Tissue Eng Part A 2011;17:255–66.
[23] Schneider CA, Rasband WS, Eliceiri KW. NIH Image to ImageJ: 25 years of image analysis. Nat Methods 2012;9:671–5.
[24] Gentleman CPaCHaR. affyQCReport: QC report generation for affyBatch objects; 2005.
[25] Gautier L, Cope L, Bolstad BM, Irizarry RA. affy–analysis of Affymetrix GeneChip data at the probe level. Bioinformatics 2004;20:307–15.
[26] Dennis Jr G, Sherman BT, Hosack DA, Yang J, Gao W, Lane HC, et al. DAVID: database for Annotation, Visualization, and Integrated discovery. Genome Biol 2003;4:P3.
[27] Gourlay CW, Ayscough KR. The actin cytoskeleton: a key regulator of apoptosis and ageing? Nat Rev Mol Cell Biol 2005;6:583–9.
[28] Ong WK, Chen HF, Tsai CT, Fu YJ, Wong YS, Yen DJ, et al. The activation of directional stem cell motility by green light-emitting diode irradiation. Biomaterials 2013;34:1911–20.
[29] Nakano K, Takaishi K, Kodama A, Mammoto A, Shiozaki H, Monden M, et al. Distinct actions and cooperative roles of ROCK and mDia in Rho small G protein-induced reorganization of the actin cytoskeleton in Madin-Darby canine kidney cells. Mol Biol Cell 1999;10:2481–91.
[30] Esparza J, Vilardell C, Calvo J, Juan M, Vives J, Urbano-Marquez A, et al. Fibronectin upregulates gelatinase B (MMP-9) and induces coordinated expression of gelatinase A (MMP-2) and its activator MT1-MMP (MMP-14) by human T lymphocyte cell lines. A process repressed through RAS/MAP kinase signaling pathways. Blood 1999;94:2754–66.
[31] Jin EJ, Park KS, Bang OS, Kang SS. Akt signaling regulates actin organization via modulation of MMP-2 activity during chondrogenesis of chick wing limb bud mesenchymal cells. J Cell Biochem 2007;102:252–61.
[32] Leinweber BD, Leavis PC, Grabarek Z, Wang CL, Morgan KG. Extracellular regulated kinase (ERK) interaction with actin and the calponin homology (CH) domain of actin-binding proteins. Biochem J 1999;344(Pt 1):117–23.
[33] Haines RL, Lane EB. Keratins and disease at a glance. J Cell Sci 2012;125:3923–8.
[34] Herrmann H, Bar H, Kreplak L, Strelkov SV, Aebi U. Intermediate filaments: from cell architecture to nanomechanics. Nat Rev Mol Cell Biol 2007;8:562–73.
[35] Goldman RD, Cleland MM, Murthy SN, Mahammad S, Kuczmarski ER. Inroads into the structure and function of intermediate filament networks. J Struct Biol 2012;177:14–23.
[36] Eriksson JE, Dechat T, Grin B, Helfand B, Mendez M, Pallari HM, et al. Introducing intermediate filaments: from discovery to disease. J Clin Invest 2009;119:1763–71.
[37] Chang L, Goldman RD. Intermediate filaments mediate cytoskeletal crosstalk. Nat Rev Mol Cell Biol 2004;5:601–13.
[38] Windoffer R, Beil M, Magin TM, Leube RE. Cytoskeleton in motion: the dynamics of keratin intermediate filaments in epithelia. J Cell Biol 2011;194:669–78.
[39] Sergi C, Abdualmjid R, Abuetabh Y. Canine liver transplantation model and the intermediate filaments of the cytoskeleton of the hepatocytes. J Biomed Biotechnol 2012;2012:131324.
[40] Reichelt J, Bussow H, Grund C, Magin TM. Formation of a normal epidermis supported by increased stability of keratins 5 and 14 in keratin 10 null mice. Mol Biol Cell 2001;12:1557–68.
[41] Joseph A, Powell-Richards AO, Shanmuganathan VA, Dua HS. Epithelial cell characteristics of cultured human limbal explants. Br J Ophthalmol 2004;88:393–8.
[42] Kloepper JE, Tiede S, Brinckmann J, Reinhardt DP, Meyer W, Faessler R, et al. Immunophenotyping of the human bulge region: the quest to define useful in situ markers for human epithelial hair follicle stem cells and their niche. Exp Dermatol 2008;17:592–609.
[43] Haque S, Haruna Y, Saito K, Nalesnik MA, Atillasoy E, Thung SN, et al. Identification of bipotential progenitor cells in human liver regeneration. Lab Invest 1996;75:699–705.
[44] Schweizer J, Bowden PE, Coulombe PA, Langbein L, Lane EB, Magin TM, et al. New consensus nomenclature for mammalian keratins. J Cell Biol 2006;174:169–74.
[45] Rogers GE. Hair follicle differentiation and regulation. Int J Dev Biol 2004;48:163–70.
[46] Gong H, Zhou H, McKenzie GW, Yu Z, Clerens S, Dyer JM, et al. An updated nomenclature for keratin-associated proteins (KAPs). Int J Biol Sci 2012;8:258–64.
[47] Sasaki M, Abe R, Fujita Y, Ando S, Inokuma D, Shimizu H. Mesenchymal stem cells are recruited into wounded skin and contribute to wound repair by transdifferentiation into multiple skin cell type. J Immunol 2008;180:2581–7.

[48] Sivamani RK, Schwartz MP, Anseth KS, Isseroff RR. Keratinocyte proximity and contact can play a significant role in determining mesenchymal stem cell fate in human tissue. FASEB J 2011;25:122–31.
[49] Wu Y, Chen L, Scott PG, Tredget EE. Mesenchymal stem cells enhance wound healing through differentiation and angiogenesis. Stem Cells 2007;25:2648–59.
[50] Aljitawi OS, Xiao Y, Zhang D, Stehno-Bittel L, Garimella R, Hopkins RA, et al. Generating CK19-positive cells with hair-like structures from Wharton's jelly mesenchymal stromal cells. Stem Cells Dev 2013;22:18–26.
[51] Hwang S, Hong HN, Kim HS, Park SR, Won YJ, Choi ST, et al. Hepatogenic differentiation of mesenchymal stem cells in a rat model of thioacetamide-induced liver cirrhosis. Cell Biol Int 2012;36:279–88.
[52] Rogers MA, Winter H, Langbein L, Bleiler R, Schweizer J. The human type I keratin gene family: characterization of new hair follicle specific members and evaluation of the chromosome 17q21.2 gene domain. Differentiation 2004;72:527–40.
[53] Durocher D, Charron F, Warren R, Schwartz RJ, Nemer M. The cardiac transcription factors Nkx2-5 and GATA-4 are mutual cofactors. EMBO J 1997;16:5687–96.
[54] Reamon-Buettner SM, Borlak J. NKX2-5: an update on this hypermutable homeodomain protein and its role in human congenital heart disease (CHD). Hum Mutat 2010;31:1185–94.
[55] Nettore IC, Cacace V, De Fusco C, Colao A, Macchia PE. The molecular causes of thyroid dysgenesis: a systematic review. J Endocrinol Invest 2013;36:654–64.
[56] Arminan A, Gandia C, Bartual M, Garcia-Verdugo JM, Lledo E, Mirabet V, et al. Cardiac differentiation is driven by NKX2.5 and GATA4 nuclear translocation in tissue-specific mesenchymal stem cells. Stem Cells Dev 2009;18:907–18.
[57] Riazi AM, Lee H, Hsu C, Van Arsdell G. CSX/Nkx2.5 modulates differentiation of skeletal myoblasts and promotes differentiation into neuronal cells in vitro. J Biol Chem 2005;280:10716–20.